

Low Arabian dust extinction-to-backscatter ratio

R. E. Mamouri,¹ A. Ansmann,² A. Nisantzi,¹ P. Kokkalis,³ A. Schwarz,² and D. Hadjimitsis¹

Received 24 July 2013; revised 19 August 2013; accepted 21 August 2013.

[1] Compared to typical values of 50–60 sr of the extinction-to-backscatter ratio (lidar ratio) at 532 nm of western Saharan mineral dust, low dust lidar ratios from 33.7±6.7 to 39.1±5.1 sr were derived from polarization lidar observations at Limassol, Cyprus (34°N, 33°E) during an outbreak of Arabian dust mainly from Syria in September 2011, indicated by particle linear depolarization ratios up to 28%–35%. The applied new polarization-lidar/photometer method for the extraction of the dust-related lidar-ratio information from the lidar data is outlined, and the results of the dust outbreak which lasted over several days are discussed. The results confirm an Aerosol Robotic Network photometer study on Arabian dust lidar ratios. **Citation:** Mamouri, R. E., A. Ansmann, A. Nisantzi, P. Kokkalis, A. Schwarz, and D. Hadjimitsis (2013), Low Arabian dust extinction-to-backscatter ratio, *Geophys. Res. Lett.*, 40, doi:10.1002/grl.50898.

1. Introduction

[2] The particle extinction-to-backscatter ratio or lidar ratio S is an important quantity in the characterization of atmospheric aerosols [Müller *et al.*, 2007; Papayannis *et al.*, 2008; Tesche *et al.*, 2011; Mamouri *et al.*, 2012]. It is also required to analyze standard backscatter lidar observations and to convert the retrieved profiles of the particle backscatter coefficient into particle extinction coefficients. The latter are used in the description of the radiative effect of aerosols (direct effect on climate). Desert dust is one of the major components of atmospheric aerosols and the Saharan and Arabian deserts are among the major dust sources of the world. A good characterization of the optical properties of Saharan and Arabian dust particles is thus a prerequisite for an adequate consideration of mineral dust particles in radiative transfer calculations [see, e.g., Heinold *et al.*, 2011]. However, Arabian dust lidar studies are rare.

[3] Recently, Schuster *et al.* [2012] showed that the illite concentration in dust particles decreases from values of about 80% in western Saharan to less than 5% in eastern Saharan and Arabian dust particles. This has a strong effect on the optical properties. Schuster *et al.* [2012] found a significant decrease of the real part of the refractive index from 1.55 for Arabian dust to 1.45 for western Saharan

dust for the 500–550 nm wavelength range. Accordingly, the lidar ratio dropped from values around 60 sr for western Saharan dust to values around 40 sr for Arabian dust as derived from column-integrated sun/sky photometer observations at 500 nm wavelength in cases with a dust fraction of more than 95%. However, comparisons of direct lidar ratio observations with Raman lidar observations indicate that the dust lidar ratio from photometer observations may be overestimated by 10%–20% [Müller *et al.*, 2012; Wagner *et al.*, 2013]. This is most probably caused by the use of a spheroidal particle model for the irregularly shaped desert dust particles in the model-based estimation of the scattering phase function at 180° scattering angle and the lidar ratio. In contrast to the lidar, the photometer is not able to directly measure particle scattering properties at 180° scattering angle. Here we present, for the first time, lidar-derived Arabian dust extinction-to-backscatter ratios and compare them with the results of Schuster *et al.* [2012]. A new polarization-lidar-based approach is applied to extract the dust-related lidar ratio information from the total aerosol backscatter and extinction properties observed with the lidar/photometer combination.

[4] In our letter, we also want to emphasize how important accompanying particle depolarization-ratio observations are to quantify the contribution of desert dust to the observed optical properties. Müller *et al.* [2007] reported lidar ratios of 38±5 sr for aged Saudi Arabian dust after long range transport to Male, Maldives. However, depolarization ratios were not measured so that it remained an open question to what extent these aged dust air masses were contaminated by nondust aerosol particles.

[5] Section 2 provides a brief overview over the lidar/photometer field site. The methodological background of the lidar retrieval procedure is given in section 3, while the results are then discussed in section 4, followed by a short summary.

2. Instrumentation

[6] The lidar station of Cyprus University of Technology (CUT) at Limassol (34°N, 33°E, 50 m above sea level, asl) is located at the south coast of the Cyprus island, about 150 km south of Turkey and 400 km west of Syria. The lidar transmits linearly polarized laser pulses at 532 nm and detects the parallel- and cross-polarized signal components. Calibration of the polarization channels is performed by rotating the box with the polarization sensitive channels following the methodology of Freudenthaler *et al.* [2009].

[7] The full overlap of the laser beam with the receiver field of view of the 20 cm Cassegrain telescope is obtained at heights around 300 m above sea level (asl) and therefore in most cases within the shallow planetary boundary layer (PBL). The overlap characteristics were checked by

¹Department of Civil Engineering and Geomatics, Cyprus University of Technology, Limassol, Cyprus.

²Leibniz Institute for Tropospheric Research, Leipzig, Germany.

³National Technical University of Athens, Athens, Greece.

Corresponding author: R. E. Mamouri, Cyprus University of Technology, Department of Civil Engineering and Geomatics, Saripolou 2-6, 3036 Achilleos 1A Building, Limassol, Cyprus. (rodanthi.mamouri@cut.ac.cy)

©2013. American Geophysical Union. All Rights Reserved.
0094-8276/13/10.1002/grl.50898

near-range Raman lidar observations at 532 and 607 nm (nitrogen Raman channel) at clear sky conditions at Limasol [Wandinger and Ansmann, 2002]. Simulations based on the specific lidar configuration with an idealized well defined laser beam divergence show the full overlap already at 250 m height. Unfortunately, Raman signals were not available for the studied September 2001 period.

[8] For the calibration of the profile of the measured 532 nm elastic backscatter signal, pure Rayleigh signals were simulated based on actual temperature and pressure profiles, and the measured 532 nm signals were fitted to the Rayleigh signal profile in the aerosol-free middle to upper troposphere. The reference total-to-particle backscatter ratio was set to 1.01 at heights around 5.5–6.0 km in the particle backscatter retrieval presented in the next section.

[9] The lidar is collocated with an Aerosol Robotic Network (AERONET, <http://aeronet.nasa.gov>) sun/sky photometer [Holben et al., 1998]. The CUT AERONET photometer allows the retrieval of the aerosol optical thickness (AOT) at 8 wavelengths from 339 to 1638 nm. Angle-dependent sky radiance observations at 4 wavelengths are performed in addition. From these measurements, the particle lidar ratio for the total tropospheric column can be derived [Dubovik et al., 2006; Schuster et al., 2012]. Comparisons with the lidar-derived lidar ratios will be discussed in section 4.

3. Method

[10] The lidar ratio is defined as the ratio of particle extinction coefficient (scattering plus absorption coefficient) to particle backscatter coefficient (180° scattering coefficient) and depends in a complex way on the particle size distribution, chemical composition of the particles and, in the case of mineral dust particles, especially from the morphological properties of the irregularly shaped desert dust particles [Müller et al., 2007, 2012; Papayannis et al., 2008].

[11] By combining sun/sky-photometer-retrieved particle optical depth τ_T at 532 nm and lidar observations of the 532 nm particle backscatter coefficient $\beta_T(z)$, the so-called column lidar ratio at 532 nm for the tropospheric column can be derived [see, e.g., Ansmann, 2006]:

$$S_T = \frac{\tau_T}{\int_{R_0}^{R_2} \beta_T(z) dz} \quad (1)$$

where R_0 and R_2 denote the bottom and top height of the troposphere, respectively.

[12] The column lidar ratio is the backscatter-weighted vertical mean lidar ratio. Thus, layers with strong backscattering, such as dust layers, dominate the column lidar ratio. The lidar return signals are analyzed with the Fernald method [Fernald, 1984] with the column lidar ratio as input. For the optimum input S_T , the particle optical depth expressed by $S_T \int_{R_0}^{R_2} \beta_T(z) dz$ matches the photometer-derived optical depth τ_T in this one-aerosol-layer approach. For the lowermost heights (below 300 m, where the overlap between laser beam and receiver field of view is incomplete), we assumed an almost well-mixed layer with a moderate, linear decrease of the particle backscatter coefficient by 10% from the surface to 300 m height during noon and afternoon hours and a linear decrease by a factor of 2 in the early

morning hours at stable atmospheric conditions. This assumption on the near-range backscatter profile is based on careful inspections of a large number of profiles of the signal ratio of the 532 nm elastic backscatter signal to the 607 nm nitrogen Raman signal. This signal ratio is essentially independent of any overlap effect.

[13] A more realistic atmospheric scenario assumes different aerosol mixtures and types (and thus different lidar ratios) in the PBL and in the free troposphere (FT). In this case, the two-layer approach of the Fernald method is applied [see, e.g., Ansmann, 2006]. Now we search for the optimum pair of column lidar ratios S_{PBL} and S_{FT} which must fulfill the following condition:

$$\tau_T = S_{PBL} \int_{R_0}^{R_1} \beta_{PBL}(z) dz + S_{FT} \int_{R_1}^{R_2} \beta_{FT}(z) dz. \quad (2)$$

In practice, one of the two lidar ratios S_{PBL} or S_{FT} must be known a priori. A good knowledge of the climatological behavior of S_{PBL} may be gathered from long-term observations of PBL lidar ratios in the absence of lofted layers. For Cyprus, typical values are around 35 sr in cases with about 50% contribution of marine particles (lidar ratio 20 sr) to particle extinction in the PBL, and another 50% contribution by urban haze (lidar ratio of 50–60 sr) according the AERONET fine-mode (urban) and coarse-mode (marine) AOT observations. When marine particles dominate, e.g., during situations with westerly winds, the lidar ratio is around 25 sr. However, the PBL AOT was of the order of 0.05 or less during the September 2011 period, and contributed <20% to the total AOT so that uncertainties in the S_{FT} values were found to be around 10% when varying the S_{PBL} by ± 10 sr.

[14] With known S_{PBL} , S_{FT} is the free parameter in the retrieval. The S_{FT} value is varied until the column-integrated backscatter-coefficient profile multiplied by the lidar-ratio step function (S_{PBL} everywhere in the PBL, S_{FT} in the free troposphere) matches the AOT measured with photometer. The results are trustworthy when the solutions of the one-layer and two-layer approaches of the Fernald method are in good agreement and do not deviate by more than 5%. This means for the column lidar ratios:

$$S_T \approx \frac{S_{PBL} \int_{R_0}^{R_1} \beta_{PBL}(z) dz}{\int_{R_0}^{R_2} [\beta_{PBL}(z) + \beta_{FT}(z)] dz} + \frac{S_{FT} \int_{R_1}^{R_2} \beta_{FT}(z) dz}{\int_{R_0}^{R_2} [\beta_{PBL}(z) + \beta_{FT}(z)] dz}. \quad (3)$$

This good agreement according to equation (3) was always obtained for the September 2011 cases discussed below.

[15] In the last step, we separate the backscatter coefficients $\beta_{FT,s}(z)$ of spherical (nondust) particles (fine mode) and $\beta_{FT,d}(z)$ of nonspherical dust particles (coarse mode) in the free troposphere by means of the polarization lidar technique [Tesche et al., 2009]. Spherical particles (e.g., anthropogenic haze, fire smoke) cause a particle depolarization ratio of 5% or less, whereas desert dust leads to depolarization ratios of 30%–35%. Highly accurate depolarization-ratio measurements are needed in the retrieval. We checked our depolarization ratios frequently by analyzing the values in the marine boundary layer where the depolarization ratio must be $\leq 5\%$ in the absence of dust. After the separation, the following relationship between the optical depth of

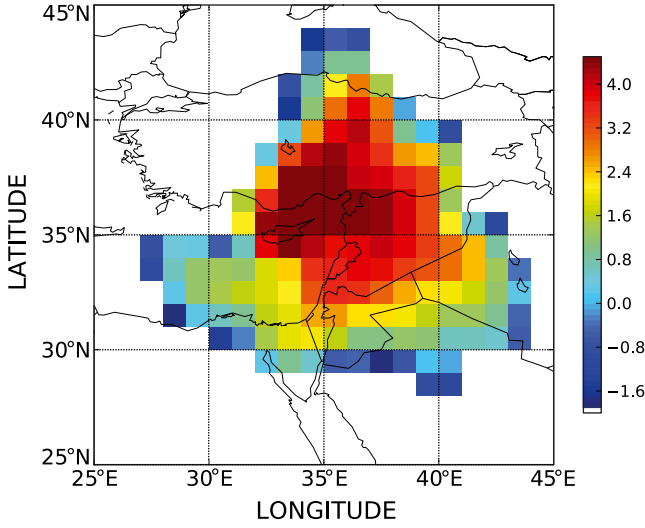


Figure 1. Source identification of the aerosol layers which crossed Limassol (34°N, 33°E) in the altitude range of the main dust layers (1000–2500 m) on 28 September 2011, 0840–0930 UTC. FLEXPART 3 day backward simulations are shown [Stohl et al., 2005]. The color coding corresponds to the logarithm of the sum of the residence time of all air parcels that have passed over a pixel (source region) between 0–2000 m height and finally reached Limassol between 1000–2500 m height.

all particles, nonspherical, and spherical particles must be fulfilled:

$$S_{FT} \int_{R_1}^{R_2} \beta_{FT}(z) dz = S_{FT,s} \int_{R_1}^{R_2} \beta_{FT,s}(z) dz + S_{FT,d} \int_{R_1}^{R_2} \beta_{FT,d}(z) dz. \quad (4)$$

Here $S_{FT,s}$ must be assumed a priori and is estimated from our long-term lidar/photometer observations of free tropospheric aerosols in the absence of desert dust. $S_{FT,s}$ values are around 60–70 sr in cases when urban haze and smoke dominate and around 40 sr during situation with westerly winds and air mass transport from the Mediterranean area. The retrieved product is finally the dust lidar ratio $S_{FT,d}$ in lofted desert-dust-laden plumes. The 5% deviation criterium must hold for equations (3) and (4) now.

[16] The uncertainty in $S_{FT,d}$ is mainly derived from the uncertainty in the assumed PBL lidar ratio S_{PBL} and the free tropospheric background (fine-mode) aerosol lidar ratio $S_{FT,s}$. By varying each of these two input lidar ratios by ± 10 sr (i.e., by performing two simulations for each input lidar ratio of the 11 cases shown in the next section), the respective mean deviation for each input lidar ratio (mean of the two deviations from the most appropriate solution) is determined and taken as the uncertainty introduced by the respective input parameter. The uncertainty in $S_{FT,d}$ is then calculated from the square root of the quadratic sum of the S_{PBL} and $S_{FT,s}$ error contributions plus a respective uncertainty term resulting from a 10% uncertainty in the separation of the dust and spherical particle components with the depolarization-ratio technique. This error computation yields an uncertainty of 10%–20% in most of the finally derived dust-related lidar ratios $S_{FT,d}$ as presented

in the following section. In our error analysis, we ignore minor contributions by signal noise, uncertainties in the required Rayleigh extinction and backscatter calculations, and in the reference total-to-particle backscatter ratio, which may increase the overall relative uncertainty by further 5%, or even 10%–15% when the reference backscatter ratio is 1.05–1.10 instead of the selected value of 1.01. We also ignore a minor impact of a few percent by the assumption of the backscatter profile slope in the lowermost 300 m.

4. Observations

[17] A major Arabian dust outbreak reached Cyprus in the morning of 28 September 2011 and lasted for 3 days. In Figure 1, we present the 3 day FLEXPART backward simulation. Shown are accumulated residence times of air masses that traveled over particle source regions within the lowermost 2000 m above ground (boundary layer) and arrived over Cyprus in the dust layer between 1000 and 2500 m on 28 September. Continental source regions that contributed most likely to the observed aerosol over Limassol are given in orange to red. We see that the air masses sampled crossed predominantly arid areas of central-eastern Turkey and desert areas of Syria before arriving over Limassol. High depolarization ratios with maximum values of 30%–35% between 1000 and 2500 m height were observed and clearly indicated the presence of a large amount of desert dust particles.

[18] Figure 2 shows the vertical profile of the particle backscatter coefficient obtained during the morning (0749–0829 UTC) of 29 September 2011. In the lowermost 500 m, northerly winds prevailed. At these conditions, a mixture of anthropogenic haze and marine particles is responsible for

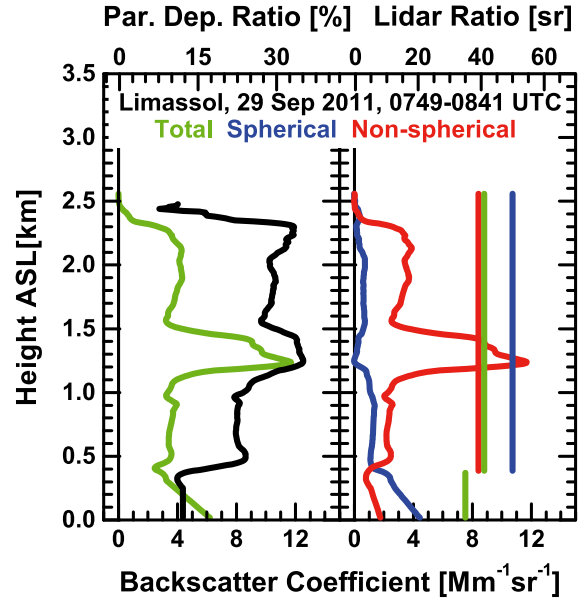


Figure 2. (left) Mean profiles (50 min) of 532 nm particle backscatter coefficient (green), particle linear depolarization ratio (black), (right) backscatter coefficient for fine-mode particles (blue) and coarse dust particles (red), and column lidar ratios for PBL (green vertical line, <350 m height) and FT (green vertical line, >350 m height), and for FT coarse dust (red vertical line) and fine-mode particles (blue vertical line).

Table 1. Retrieved and Assumed Parameters From Lidar and Photometer Observations for 11 Time Periods on 28–30 September 2011^a

Date	Time (UTC)	PBL Top (m)	S_T (sr)	$S_{T,A}$ (sr)	S_{PBL} (sr)	S_{FT} (sr)	$S_{FT,s}$ (sr)	$S_{FT,d}$ (sr)
28 Sep 2011	0742–0841	310	47	44	35	49	60	37.1±13.5
	0842–0929	310	42		35	43	60	33.7±6.7
	0929–1019	310	40	46	35	40	50	34.9±6.5
29 Sep 2011	0749–0829	350	40	43	35	41	50	39.1±5.1
	0829–0929	310	38		35	38	50	34.9±5.9
	0929–1028	310	37		30	38	50	33.8±5.8
	1028–1101	310	39	46	30	40	50	34.4±7.4
30 Sep 2011	0842–0929	350	39	41	25	42	50	38.2±7.4
	0929–1029	310	35		25	38	40	36.8±8.0
	1029–1144	350	36	32	25	38	40	35.8±13.0
	1144–1226	350	36		25	38	40	35.8±11.9

^aListed are the top height of the PBL, column lidar ratios S_T (after equation (3)) and $S_{T,A}$ (532 nm, from AERONET data), S_{PBL} (assumed PBL lidar ratio), S_{FT} (FT column lidar ratio, equation (4)), $S_{FT,s}$ (assumed FT lidar ratio of nondust particles, equation (4)), and $S_{FT,d}$ (retrieved FT lidar ratio of coarse dust, equation (4)).

aerosol backscattering and extinction in the almost 400 m deep PBL. The 532 nm PBL AOT derived from the column backscatter coefficient (multiplied by the assumed S_{PBL} value of 35 sr) was 0.06. The total (PBL + FT) AOT was 0.43. Thus, the lofted aerosol contributed about 85% to the total AOT.

[19] From Figure 2, one can see that the lofted desert dust layer extended from 500 to 2500 m. The particle depolarization ratio was >25% for heights >1300 m and reached a maximum value of 35% in the strongest dust layer. A maximum value of the particle backscatter coefficient of $12 \text{ M m}^{-1} \text{ sr}^{-1}$ was observed and pointed to particle extinction coefficients of about 500 M m^{-1} . The AERONET photometer observations showed a clear bimodal size distribution with a strong coarse mode. Fine-mode and coarse-mode effective radii were 0.12 and $2 \mu\text{m}$, respectively.

[20] The separation into fine-mode and coarse-mode backscatter coefficients in Figure 2, right indicates the presence of dust particles throughout the troposphere up to 2500 m height. The FT AOT caused by coarse-mode dust particles was 0.28 and contributed about 65% to the total AOT and about 85% to the FT AOT. Correspondingly, the coarse-dust lidar ratio $S_{FT,d}$ of 39 sr (after equation (4)) is close to the FT lidar ratio S_{FT} . The uncertainties in our retrieval products shown in Figure 2 are small. Even if we assume a much lower or larger lidar ratio of $S_{PBL} = 20$ sr or 50 sr instead of 35 sr for the polluted marine boundary layer, the dust lidar ratio and the overall FT lidar ratio will change by no more than ± 4 sr.

[21] Table 1 and Figure 3 provide an overview of all observations and the required lidar ratio assumptions. The assumed boundary layer lidar ratios S_{PBL} were carefully selected after studying the meteorological situation. A high value of 35 sr was selected in the case of northerly winds so that the marine impact was comparably low. A lower value of 25 sr was taken during sea breeze events or when strong westerly winds and thus marine particles prevailed in the boundary layer, as was the case on 30 September. According to Table 1 and Figure 3, all observations with strong dust impact (from 28 September, case 2, to 30 September, case 1) indicate desert dust lidar ratios around 35–40 sr.

[22] In Table 1, a few AERONET-derived column lidar ratios $S_{T,A}$ are shown. We used the AERONET-derived lidar ratios at 675 and 1021 nm to extrapolate the values for

532 nm as given in Table 1. The rather weak wavelength dependence (1–3 sr larger 532 nm than 675 nm values) for the days with heavy desert dust load is in good agreement with the lidar-ratio spectral slope presented by Schuster *et al.* [2012]. The derived $S_{T,A}$ values are in reasonable agreement with the lidar-derived column lidar ratios.

[23] Schuster *et al.* [2012] found values of 37–45 sr over AERONET sites in the Arabian desert area for cases with almost negligible fine-mode contribution to AOT. Our dust-related lidar ratios $S_{FT,d}$ values are slightly lower by about 10% which is in agreement with more direct comparisons of Raman lidar and photometer observations [Müller *et al.*, 2012; Wagner *et al.*, 2013] and may be related to the used spheroidal particle model in the AERONET retrieval.

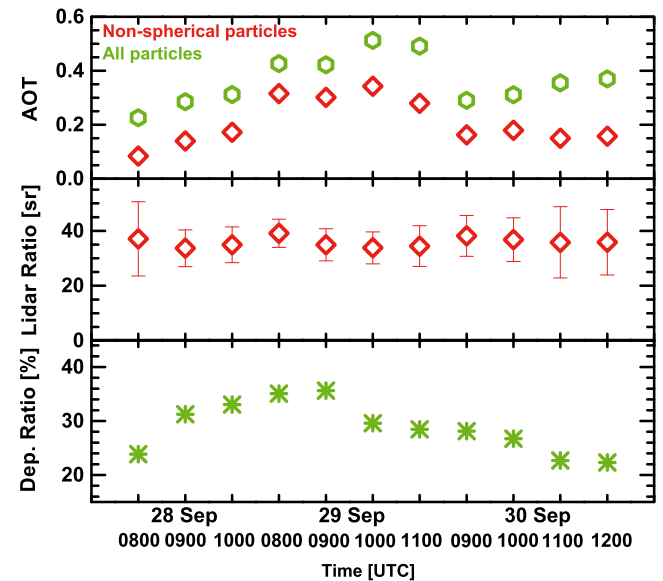


Figure 3. Overview of observed dust optical properties for the period from 28–30 September 2011. (top) Tropospheric AOT (green) and coarse-mode dust FT AOT (red). (middle) FT dust lidar ratio $S_{FT,d}$ with one-standard-deviation error bar. (bottom) Observed maximum FT particle linear depolarization ratio.

5. Summary

[24] The letter covered three important points: (1) Further evidence is provided that the extinction-to-backscatter ratio for Arabian desert dust is significantly lower than respective lidar ratios for western Saharan dust particles. Our lidar study corroborates the findings of Schuster *et al.* [2012] (modeled dust lidar ratios). (2) Because lidars provide directly measured information on 180° scattering, the combined lidar/photometer retrieval method applied here does not depend on critical assumptions (spheroidal dust particle model). (3) The importance of polarization lidar measurements for the retrieval of dust-related lidar ratio was demonstrated. Without depolarization ratio information, dust lidar ratios cannot be quantified properly because the influence of non-dust aerosol components remains unknown.

[25] **Acknowledgments.** This research forms part of the project Webair-2 funded by the Cyprus Promotion Research Foundation (CPRF). The FNL data as input for FLEXPART simulations are provided by the CISL (Computational Information Systems Laboratory) Research Data Archive (<http://rda.ucar.edu/>). The authors thank the EARLINET and ACTRIS partners, and the CUT Remote Sensing Laboratory for their support. Finally, we are grateful to AERONET for high-quality sun/sky photometer measurements.

[26] The Editor thanks two anonymous reviewers for their assistance in evaluating this paper.

References

- Ansmann, A. (2006), Ground-truth aerosol lidar observations: Can the Klett solutions obtained from ground and space be equal for the same aerosol scenario?, *Appl. Opt.*, *45*, 3367–3371.
- Dubovik, O., et al. (2006), Application of spheroid models to account for aerosol particle nonsphericity in remote sensing of desert dust, *J. Geophys. Res.*, *111*, D11208, doi:10.1029/2005JD006619.
- Fernald, F. G. (1984), Analysis of atmospheric lidar observations: Some comments, *Appl. Opt.*, *23*, 652–653.
- Freudenthaler, V., et al. (2009), Depolarization-ratio profiling at several wavelengths in pure Saharan dust during SAMUM 2006, *Tellus B*, *61*, 165–179.
- Heinold, B., I. Tegen, S. Bauer, and M. Wendisch (2011), Regional modelling of Saharan dust and biomass-burning smoke—part 2: Direct radiative forcing and atmospheric dynamic response, *Tellus B*, *63*, 800–813, doi:10.1111/j.1600-0889.2011.00574.x.
- Holben, B. N., et al. (1998), AERONET—A federated instrument network and data archive for aerosol characterization, *Remote Sens. Environ.*, *66*, 1–16.
- Mamouri, R. E., et al. (2012), Multiwavelength Raman lidar, sun photometric and aircraft measurements in combination with inversion models for the estimation of the aerosol optical and physico-chemical properties over Athens, Greece, *Atmos. Meas. Tech.*, *5*, 1793–1808, doi:10.5194/amt-5-1793-2012.
- Müller, D., A. Ansmann, I. Mattis, M. Tesche, U. Wandinger, D. Althausen, and G. Pisani (2007), Aerosol-type-dependent lidar-ratios observed with Raman lidar, *J. Geophys. Res.*, *112*, D16202, doi:10.1029/2006JD008292.
- Müller, D., et al. (2012), Comparison of optical and microphysical properties of pure Saharan mineral dust observed with AERONET Sun photometer, Raman lidar, and in situ instruments during SAMUM 2006, *J. Geophys. Res.*, *117*, D07211, doi:10.1029/2011JD016825.
- Papayannis, A., et al. (2008), Systematic lidar observations of Saharan dust over Europe in the frame of EARLINET (2000–2002), *J. Geophys. Res.*, *113*, D10204, doi:10.1029/2007JD009028.
- Schuster, G. L., M. Vaughan, D. MacDonnell, W. Su, D. Winker, O. Dubovik, T. Lapyonok, and C. Trepte (2012), Comparison of CALIPSO aerosol optical depth retrievals to AERONET measurements, and a climatology for the lidar ratio of dust, *Atmos. Chem. Phys.*, *12*, 7431–7452, doi:10.5194/acp-12-7431-2012.
- Stohl, A., C. Forster, A. Frank, P. Seibert, and G. Wotawa (2005), Technical note: The Lagrangian particle dispersion model FLEXPART version 6.2, *Atmos. Chem. Phys.*, *5*, 2461–2474, doi:10.5194/acp-5-2461-2474.
- Tesche, M., A. Ansmann, D. Müller, D. Althausen, R. Engelmann, V. Freudenthaler, and S. Groß (2009), Separation of dust and smoke profiles over Cape Verde by using multiwavelength Raman and polarization lidars during SAMUM 2008, *J. Geophys. Res.*, *114*, D13202, doi:10.1029/2009JD011862.
- Tesche, M., S. Groß, A. Ansmann, D. Müller, D. Althausen, V. Freudenthaler, and M. Esselborn (2011), Profiling of Saharan dust and biomass-burning smoke with multiwavelength polarization Raman lidar at Cape Verde, *Tellus B*, *63*, 649–676, doi:10.1111/j.1600-0889.2011.00548.x.
- Wagner, J., A. Ansmann, U. Wandinger, P. Seifert, A. Schwarz, M. Tesche, A. Chaikovsky, and O. Dubovik (2013), Evaluation of the Lidar/Radiometer Inversion Code (LIRIC) to determine microphysical properties of volcanic and desert dust, *Atmos. Meas. Tech.*, *6*, 1707–1724, doi:10.5194/amt-6-1707-2013.
- Wandinger, U., and A. Ansmann (2002), Experimental determination of the lidar overlap profile with Raman lidar, *Appl. Opt.*, *41*, 511–514.

Author Query Form

Journal: Geophysical Research Letters

Article: GRL_50898

Dear Author,

During the copyediting of your paper, the following queries arose. Please respond to these by annotating your proofs with the necessary changes/additions.

- If you intend to annotate your proof electronically, please refer to the E-annotation guidelines.
- If you intend to annotate your proof by means of hard-copy mark-up, please refer to the proof mark-up symbols guidelines. If manually writing corrections on your proof and returning it by fax, do not write too close to the edge of the paper. Please remember that illegible mark-ups may delay publication.

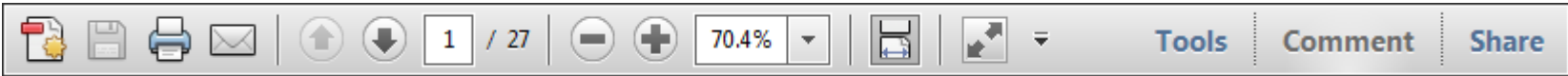
Whether you opt for hard-copy or electronic annotation of your proofs, we recommend that you provide additional clarification of answers to queries by entering your answers on the query sheet, in addition to the text mark-up.

Query No.	Query	Remark
Q1	AUTHOR: As per AGU style, department is required in university affiliations. Please supply department for “National Technical University of Athens”.	

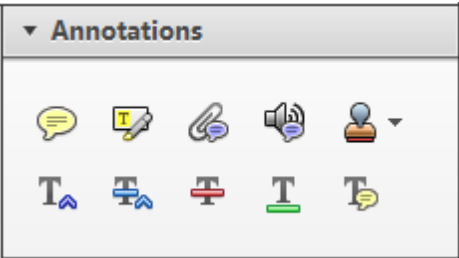
USING e-ANNOTATION TOOLS FOR ELECTRONIC PROOF CORRECTION

Required software to e-Annotate PDFs: Adobe Acrobat Professional or Adobe Reader (version 7.0 or above). (Note that this document uses screenshots from Adobe Reader X)
The latest version of Acrobat Reader can be downloaded for free at: <http://get.adobe.com/uk/reader/>

Once you have Acrobat Reader open on your computer, click on the [Comment](#) tab at the right of the toolbar:



This will open up a panel down the right side of the document. The majority of tools you will use for annotating your proof will be in the [Annotations](#) section, pictured opposite. We've picked out some of these tools below:



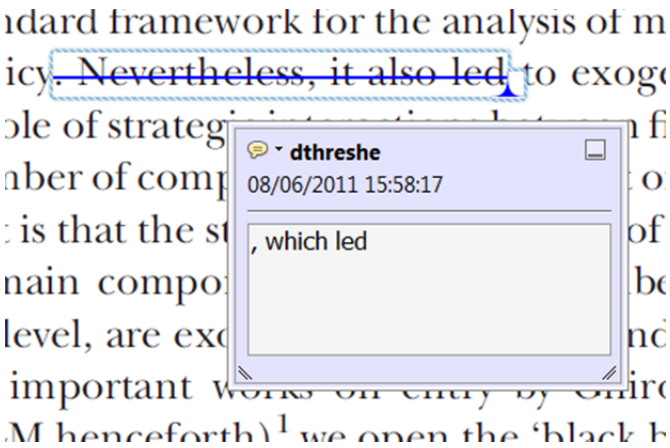
1. [Replace \(Ins\)](#) Tool – for replacing text.



Strikes a line through text and opens up a text box where replacement text can be entered.

How to use it

- Highlight a word or sentence.
- Click on the [Replace \(Ins\)](#) icon in the Annotations section.
- Type the replacement text into the blue box that appears.



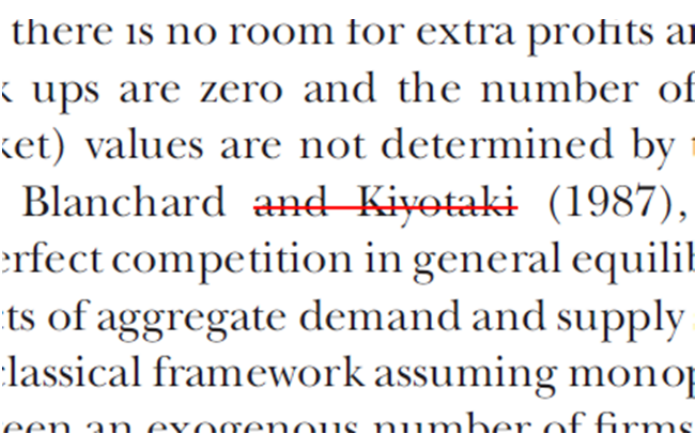
2. [Strikethrough \(Del\)](#) Tool – for deleting text.



Strikes a red line through text that is to be deleted.

How to use it

- Highlight a word or sentence.
- Click on the [Strikethrough \(Del\)](#) icon in the Annotations section.



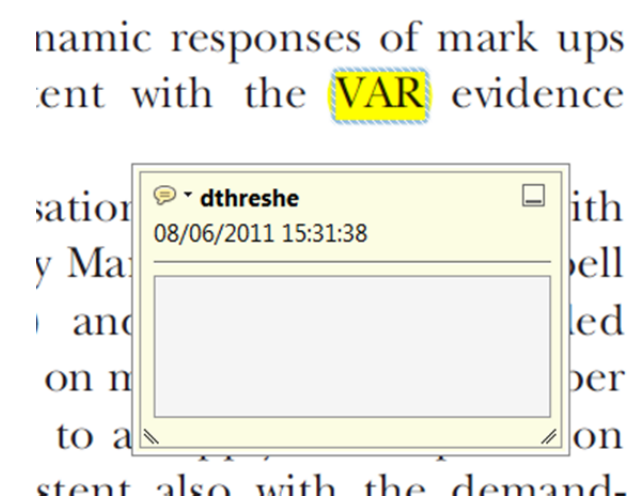
3. [Add note to text](#) Tool – for highlighting a section to be changed to bold or italic.



Highlights text in yellow and opens up a text box where comments can be entered.

How to use it

- Highlight the relevant section of text.
- Click on the [Add note to text](#) icon in the Annotations section.
- Type instruction on what should be changed regarding the text into the yellow box that appears.



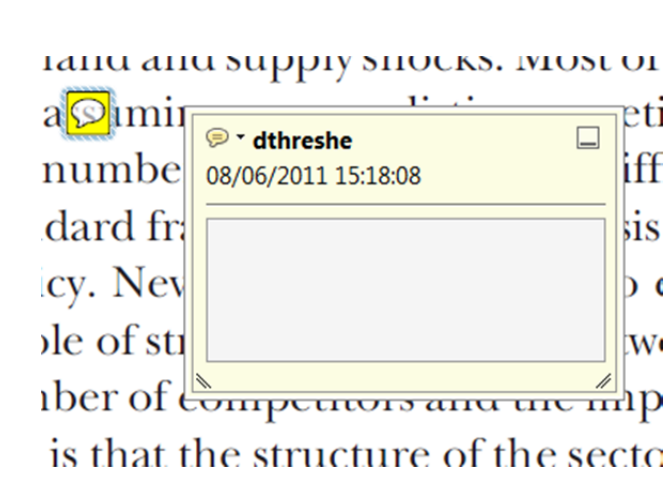
4. [Add sticky note](#) Tool – for making notes at specific points in the text.



Marks a point in the proof where a comment needs to be highlighted.

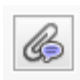
How to use it

- Click on the [Add sticky note](#) icon in the Annotations section.
- Click at the point in the proof where the comment should be inserted.
- Type the comment into the yellow box that appears.



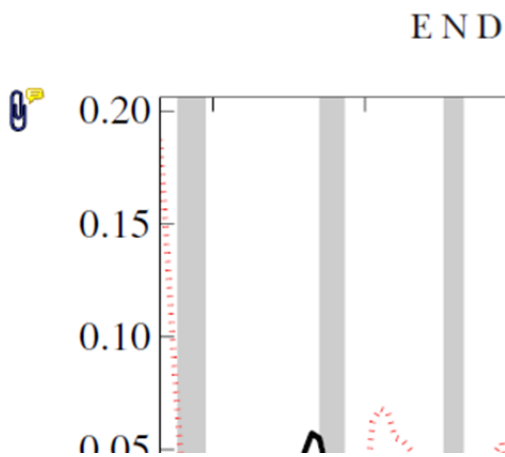
USING e-ANNOTATION TOOLS FOR ELECTRONIC PROOF CORRECTION

5. **Attach File** Tool – for inserting large amounts of text or replacement figures.


 Inserts an icon linking to the attached file in the appropriate place in the text.

How to use it

- Click on the **Attach File** icon in the Annotations section.
- Click on the proof to where you'd like the attached file to be linked.
- Select the file to be attached from your computer or network.
- Select the colour and type of icon that will appear in the proof. Click OK.



6. **Add stamp** Tool – for approving a proof if no corrections are required.

 Inserts a selected stamp onto an appropriate place in the proof.

How to use it

- Click on the **Add stamp** icon in the Annotations section.
- Select the stamp you want to use. (The **Approved** stamp is usually available directly in the menu that appears).
- Click on the proof where you'd like the stamp to appear. (Where a proof is to be approved as it is, this would normally be on the first page).

of the business cycle, starting with the
on perfect competition, constant return
production. In this environment goods
extra profits and the structure of market
he number of firms in the individual firm
etermined by the model. The New-Key
otaki (1987), has introduced product
general equilibrium models with nomin
ed and supply shocks. Most of this literat

APPROVED

Drawing Markups

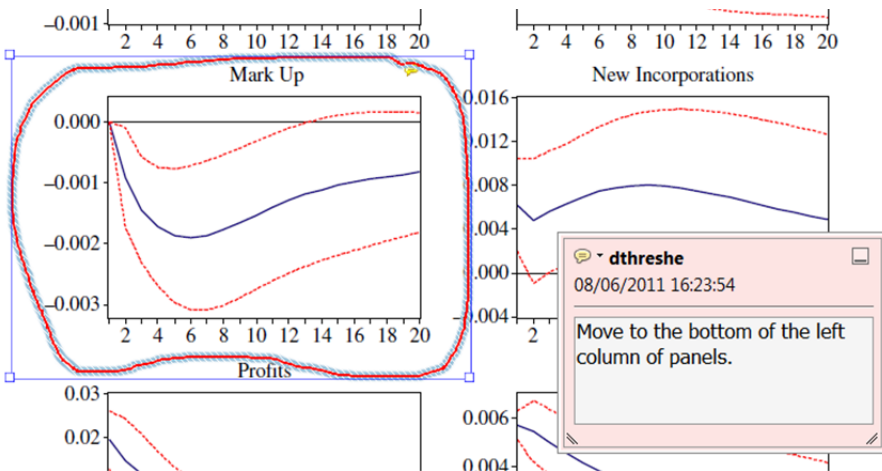


How to use it

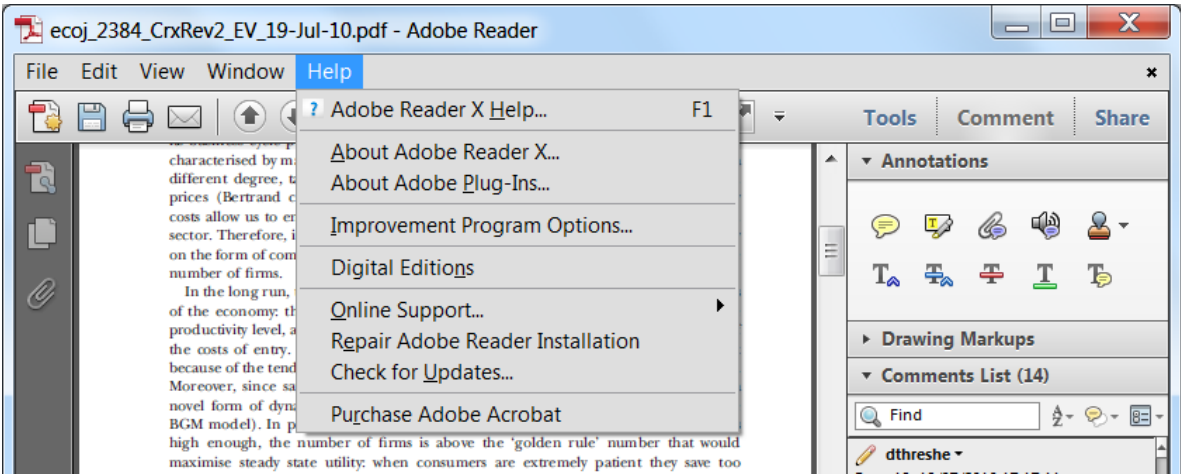
- Click on one of the shapes in the **Drawing Markups** section.
- Click on the proof at the relevant point and draw the selected shape with the cursor.
- To add a comment to the drawn shape, move the cursor over the shape until an arrowhead appears.
- Double click on the shape and type any text in the red box that appears.

7. **Drawing Markups** Tools – for drawing shapes, lines and freeform annotations on proofs and commenting on these marks.

Allows shapes, lines and freeform annotations to be drawn on proofs and for comment to be made on these marks..



For further information on how to annotate proofs, click on the **Help** menu to reveal a list of further options:





Additional reprint and journal issue purchases

Should you wish to purchase additional copies of your article, please click on the link and follow the instructions provided:
<https://caesar.sheridan.com/reprints/redir.php?pub=10089&acro=GRL>

Corresponding authors are invited to inform their co-authors of the reprint options available.

Please note that regardless of the form in which they are acquired, reprints should not be resold, nor further disseminated in electronic form, nor deployed in part or in whole in any marketing, promotional or educational contexts without authorization from Wiley. Permissions requests should be directed to mailto: permissionsus@wiley.com

For information about 'Pay-Per-View and Article Select' click on the following link: <http://wileyonlinelibrary.com/ppv>